ORIGINAL RESEARCH ARTICLE

Electrodeposited Ni-Cu Coatings with Hierarchical Surface Morphology

S. STAROŃ, P. LEDWIG, and B. DUBIEL

In recent years, Ni-Cu alloy coatings obtained by electrolytic deposition have received increasing interest, because of their good anti-corrosive, mechanical, magnetic, electrical, and decorative properties. Further applications of these coatings for electrode materials and catalysts may be possible by developing hierarchical surface morphology, and thus a combination of high surface roughness, high microhardness, and good corrosion resistance. In the present work, four types of Ni-Cu alloy coatings were deposited in a single-step process from electrolytic baths with Cu^{2+}:Ni^{2+} concentrations equal to 1:30, 1:20, 1:15, and 1:10 using deposition current densities of 2 A/dm^2 and 4 A/dm^2. The surface morphology of the coatings was characterized using a scanning electron microscope and an optical profilometer. The coatings exhibited a nodular morphology, which with the change of the Cu^{2+}:Ni^2 ratio and the current parameters changed from smooth and compact to rougher with regularly spaced nodular microprotrusions. Thus, a hierarchical surface morphology was obtained. Transmission electron microscopy investigations revealed that the fine-grained microstructure of the coatings consisted of the γ solid solution, as well as the metastable intermetallic $L1_0$ NiCu phase. The differences in the Cu concentration at the cross-sections demonstrated by quantitative microanalysis of the chemical composition indicated a dendritic growth of the coatings and a preferential reduction of copper ions over nickel ions. The coatings were also characterized by a microhardness greater than 3.71 GPa and good electrochemical corrosion resistance in chloride media. Coatings with hierarchical morphology and high surface roughness showed a higher corrosion current. The study provides a new method for electrodeposition hierarchical Ni-Cu coatings under specific chemical compositions of the electrolytic bath and current conditions, characterized by a combination of promising properties for electrode and catalytic applications.

S. STAROŃ, P. LEDWIG, and B. DUBIEL are with the Faculty of Metals Engineering and Industrial Computer Science, AGH University of Science and Technology, al. Adama Mickiewicza 30, 30-059 Kraków, Poland. Contact e-mail: pledwig@agh.edu.pl

Manuscript submitted November 23, 2021; accepted March 6, 2022.
Article published online March 29, 2022

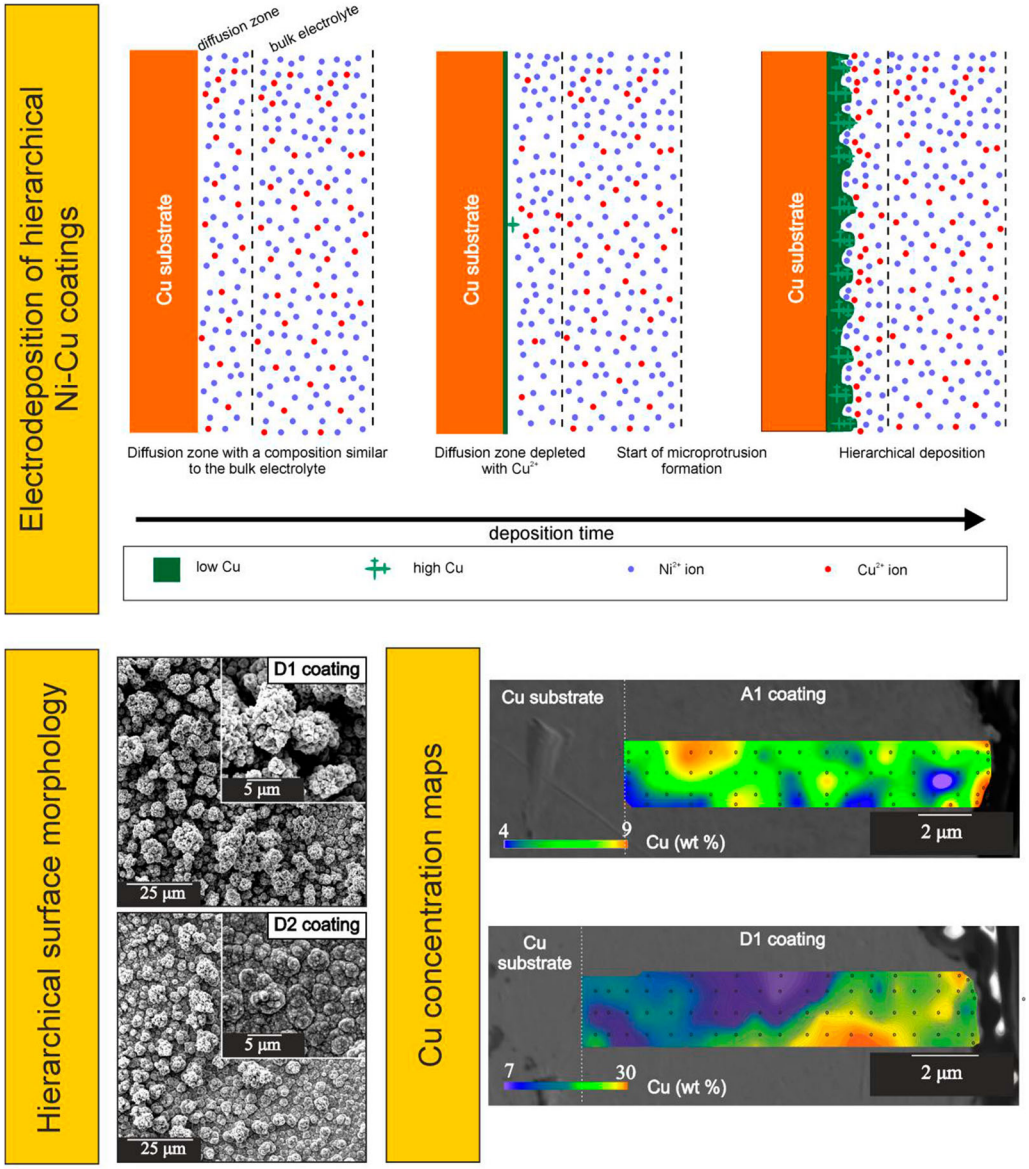

https://doi.org/10.1007/s11661-022-06649-7
© The Author(s) 2022

I. INTRODUCTION

ONE of the most popular methods for obtaining Ni-Cu coatings is electrolytic deposition. The main advantage of the process is the ability to control the chemical composition and structure of the coatings by changing the current density,[1,2] the deposition potential,[3,4] the pH, as well as the chemical composition of the electrolytic bath.[2,3,5–10] By modifying the process parameters, it is possible to order the distribution of morphological features on the surface and consequently shape the hierarchical coating morphology. To obtain this, the electrodeposition with dynamic hydrogen bubble template (DHBT),[11–13] electrodeposition under super gravity field,[14] electrolytic bath modification by chemical growth modifier,[12,15] or deposition under specific current conditions[16–18] could be used.

Ni-Cu alloy coatings are characterized primarily by good corrosion resistance and mechanical, decorative, optical, electrocatalytic, thermoelectric, and magnetic properties.[2,3,5] As a result of their excellent optical properties and good electrical conductivity, Ni-Cu alloys are used as modules for mirror telescopes and other astronomical instruments.[5] Electrodeposited Ni-Cu alloys are also used as supercapacitors.[19,20] Thanks to the high corrosion resistance as well as good

thermal and electrical conductivity, electrodeposited Ni-Cu alloys are also used in the marine, oil, and gas industries and sanitary engineering. The possibility of obtaining materials with high surface development makes Ni-Cu alloys used as oxygen/hydrogen evolution reaction electrodes (OER/HER),[21] superhydrophobic coatings,[22] and radiators in microelectronic applications.[23] To meet the increasing demand for catalysts and OER/HER electrodes with more effective charge transport during reactions, materials with a 3D hierarchical structure can be applied.[24] One of the methods that allows production of Ni-Cu coatings with a hierarchical structure is electrochemical deposition.

Co-deposition of Cu and Ni is strongly dependent on the deposition potential, as it influences the chemical composition, microstructure, and surface morphology of Ni-Cu alloys. At lower potential values, the alloys are enriched with nickel, and the surface morphology changes from dendritic to cauliflower-like. The increase in the relative concentration of Ni^{2+} ions in the bath leads to an increase in the Ni content in the coating, which is associated with the formation of a smooth surface.[25–27] Meanwhile, when the pH value of the bath decreases and the Cu^{2+} concentration increases, the surface roughness increases. Appropriate selection of the chemical composition of the electrolytic bath and current conditions of electrodeposition should allow the obtaining of Ni-Cu coatings with hierarchical surface morphology.

Despite many experimental results on electrodeposited Ni-Cu alloy coatings in the literature, there is limited information on their hierarchical surface morphology. However, the hierarchical Ni-Cu coatings with a larger specific surface are of great interest regarding their potential application for catalysts and electrodes.

Goranova *et al.*[18] examined Ni-Cu coatings from the baths with a high Cu^{2+}:Ni^{2+} ratio in the range from 1:2 to 1:8. They have achieved coatings with a dendritic surface morphology showing hierarchical distribution. Moreover, they proposed a numerical model of the electrodeposition based on the kinetics of co-deposition of Ni and Cu ions and the dendritic growth mechanism of two phases, namely Ni-based and Cu-based solid solutions. However, the differences in chemical composition of both phases were shown only for the subsurface areas of the coating.

Meanwhile, the range of compositions with a low Cu content has been poorly investigated, so the minimum concentration of Cu^{2+} ions needed to deposit the hierarchical Ni-Cu hierarchical coatings has not been determined. Therefore, in this work, we present the method of electrodeposition of Ni-Cu coatings with hierarchical structure from the electrolytic baths with Cu^{2+}:Ni^{2+} ratio opposite to that reported in literature.[18] We show for which Cu^{2+}:Ni^{2+} ratio the hierarchical growth begins and how the change of ions concentration influence of the growth of the coatings.

The surface morphology is influenced by many parameters of electrodeposition, among others chemical composition and pH of the electrolytic bath, current density, or temperature. In this paper, we investigate the influence of Cu^{2+}:Ni^{2+} ratio and current density on the hierarchical growth of Ni-Cu coatings. It is demonstrated that the coatings characterized by regularly spaced globular microprotrusions are deposited as a consequence of the difference in the kinetics of Ni^{2+} and Cu^{2+} electroreduction. The influence of electrodeposition conditions on the surface morphology and roughness, microstructure, chemical and phase composition, microhardness, and electrochemical properties is investigated.

II. MATERIALS AND METHODS

Four electrolytic baths with different concentrations of copper sulfate and nickel sulfate, A, B, C, and D, were used in the experiment. Cu concentrations ranging from low to high were designated to examine the influence of a high range of Cu^{2+}:Ni^{2+} ratio on the morphology, microstructure, and coating properties. The sodium citrate was added as a buffering and complexing agent. The chemical compositions of the baths are given in Table I.

The electrodeposition process was carried out using Autolab PGSTAT 302N potentiostat/galvanostat (Metrohm, Switzerland), operating with three electrodes: the working electrode (Cu substrate), the reference electrode (saturated Ag/AgCl), and the counter electrode (platinum plate). The distance between the working electrode and the counter electrode was set at 25 mm. Rectangular Cu plates with dimensions 15 mm × 25 mm × 1 mm were used as working electrodes. They were ground with water sandpapers up to 2000 grit and polished on microfiber cloth using an Al_2O_3 suspension. The pH of the electrolytic bath was equal to 4.5 ± 0.1. Deposition was carried out from freshly prepared electrolytic baths at the temperature of 25 °C with a current density equal to 2 A/dm^2 (coatings A1, B1, C1 and D1) or 4 A/dm^2 (coatings A2, B2, C2 and D2).

The electrodeposition current densities of 2 A/dm^2 and 4 A/dm^2 are within the range of values commonly used for the electrodeposition of Ni-based coatings. Through examining the deposition with different values of current density, it was possible to determine the effect of the ion electroreduction rate on the formation of hierarchical structures. A constant charge density equal to 36 °C/cm^2 was used. The variants of electrodeposited coatings and the deposition parameters are presented in Table II.

The roughness parameters were determined using an optical profilometer from VeecoWyko NT930. For each coating, an area equal to 1.235 mm^2 was measured and the R_a (arithmetical mean deviation of the roughness profile), R_q (root-mean-square deviation of the roughness profile), and R_t (maximum height of the roughness profile) parameters were determined.

Microhardness was measured using a Tukon 2500 microhardness tester (Wolpert Wilson, USA) with the Knoop indenter under a load equal to 0.025 N. The applied force was chosen such that the load did not

Table I. Chemical Composition of Electrolytic Baths

Type of bath	Cu^{2+}:Ni^{2+} Ratio	Compound [g/L]		
		$NiSO_4 \cdot 6H_2O$	$CuSO_4 \cdot 5H_2O$	$C_6H_5Na_3O_7$
A	1:30	157.8	3.2	60.0
B	1:20	157.8	4.8	60.0
C	1:15	157.8	6.4	60.0
D	1:10	157.8	9.6	60.0

Table II. Parameters of Electrolytic Deposition of Ni-Cu Alloy Coatings

Coating	Electrolyte Bath	Current Density [A/dm^2]	Deposition Time [s]
A1	A	2	1800
A2	A	4	900
B1	B	2	1800
B2	B	4	900
C1	C	2	1800
C2	C	4	900
D1	D	2	1800
D2	D	4	900

affect the substrate. Ten measurements were performed for each coating, and the microhardness (HK) was determined using Eq. [1]:

$$HK = 14.228 \cdot \frac{0.102L}{d^2} \quad [1]$$

where L and d were the load and length of the longer diagonal of hardness imprint. The Knopp hardness values were converted to GPa.

The surface morphology investigation and analysis of the chemical composition were carried out using an Inspect S50 (FEI, USA) scanning electron microscope (FEI, USA) equipped with an Octane Energy dispersive X-ray Spectroscopy detector (EDS) and Genesis software with ExpertID plugin (EDAX INC, USA). For microstructural studies the accelerating voltage from 10 to 15 kV was used, while the EDS measurements were carried out at 5 kV. The advantage of performing chemical microanalysis at low voltage is the short electron penetration depth and thus improvement of the spatial resolution. The depth of electron penetration in Ni-Cu at a 5 kV accelerating voltage calculated using the method described by Potts[28] was equal to 0.13 μm. Routinely, for quantitative EDS microanalysis, the K-α peaks of Ni at 7.471 keV and Cu at 8.040 keV spectral lines are used. At low voltage conditions, these peaks are not detected; therefore, quantification with the use of L-α peaks has to be performed. However, due to the small difference in the energy of Ni L-α (at 0.851 keV) and Cu L-α (at 0.930 keV), the peaks overlap. Being aware of this limitation, a Bayesian deconvolution approach of overlapping peaks was used. Each EDS spectrum was collected for at least 50 seconds to obtain the peak-to-background ratio of at least 2:1. The relative error of the quantitative analysis related to the overlapping of the peaks was in the range from 20 to 33 pct. To obtain quantitative chemical composition maps, EDS spectra were acquired at least a 45-point mesh on the cross-sections of the coatings. The distance between two adjacent EDS measurements was approximately 0.5 μm. Based on the results of quantitative EDS microanalysis, the chemical composition maps were generated with the use of the Surfer software (Golden Software, USA). The average Cu concentration in the coatings was calculated as the average value of the Cu concentration for all point EDS measurements used to create the map.

Microstructural investigations were performed using the JEM-2010 ARP (Jeol, Japan) transmission electron microscope (TEM). Equivalent circular diameters (ECD) of grains were calculated using ImageJ software from TEM images. The grains in the D1 and D2 coatings were manually marked on the images, and subsequently their areas and ECDs were determined.

The JEMS v4.4230 software (Pierre Stadelmann, JEMS-SAS, Switzerland) was used to analyze the selected area electron diffraction (SAED) patterns. Phase crystallographic data were taken from the Inorganic Material Database.[29]

Electrochemical corrosion measurements were carried out in 3 pct NaCl solution.

A potentiostat/galvanostat with the same system as for coating electrodeposition was used. Linear polarization was performed in a potential range from − 0.3 to 0.8 V versus Open Electrode Potential (OCP) and a scan rate equal to 0.001 V/s. If the maximum current range (0.01 A) was achieved, the measurement was shortened. For each coating, the OCP and polarization curves were

determined using Nova 2.0 software. The corrosion potential and the corrosion current density were determined by the Tafel extrapolation method.

III. RESULTS AND DISCUSSION

A. *Surface Morphology and Roughness*

Figure 1(a) through (h) shows SEM images of the surface morphology of electrodeposited Ni-Cu alloy coatings. The surface of all coatings exhibits typical nodular morphology. However, significant differences in the size and distribution of nodules occur with increasing the Cu^{2+} concentration in the electrolyte. For both investigated current densities, we observed the evolution of the surface morphology and the formation of a greater number of microprotrusions due to an increase in the concentration of Cu^{2+} ions in the electrolytic bath. In addition, the higher number of microprotrusions was noticeable for the current density of 4 A/dm^2 than for 2 A/dm^2. The surface of A1 coatings is rather smooth with sparsely located small cauliflower-like islands (Figure 1(a)). As the concentration of Cu^{2+} increases, a greater number of isolated islands are observed in B1 (Figure 1(c)), while in C1 (Figure 1(e)), the islands overlapped, but smooth areas below the coating islands were also visible. The surface morphology of D1 (Figure 1(g)) consisted of microprotrusions of a large amount of irregular surface structures in the pillar shape. Similar observations of changes in surface morphology were also observed for the deposition current of 4 A/dm^2, while the number of cauliflower islands was definitely greater than for coatings deposited at a lower current density. For a higher current density, overlapping of the islands was observed for B2 (Figure 1(d)), while C2 (Figure 1(f)) consisted of uniformly distributed cauliflower islands on the whole surface.

The literature reports that the reason for the development of a pillar morphology is a dendritic structure and may be achieved by an increase in the copper content in the deposited coatings.[18,27,30] Other researchers obtained the nodular morphology of the Ni-Cu coatings, but the pillar shape morphology has rarely been observed.[3,4,6,31–33]

Surface morphology studies by SEM were supplemented with roughness measurements. The roughness maps obtained with the use of an optical profilometer are given in Figures 2(a) through (h) and the values of roughness parameters are listed in Table III. The roughness parameters were in good agreement with the SEM observation and correlated with the type of surface morphology. The average roughness of the coatings is strictly dependent on the surface morphology of the Ni-Cu coatings. The lowest R_a values were observed for the A1 and A2 coatings due to the presence of a smooth surface with a low number of small microprotrusions. A slightly higher R_a characterized the B2 and C1 coatings, which showed a surface morphology consisting of overlapped cauliflower islands. In turn, C2 and D2 coatings with surface morphology consisting of homogeneously distributed cauliflower islands were characterized by even higher R_a values. The D1 coating, which consisted of a large amount of irregular surface structures, microprotrusions of pillar shape, had the highest R_a value.

The increase in R_t values was due to the increase in the concentration of Cu^{2+} ions for both investigated current densities. The coatings deposited at 4 A/dm^2 were characterized by the presence of microprotrusions higher than those electrodeposited under 2 A/dm^2.

The results of the roughness measurements confirmed that the presence of pillar shapes and cauliflower-like microprotrusions was associated with a rough surface. Based on roughness profiles, it was possible to estimate the heights of single or/and colonies of morphological features using the procedure described in.[16] For the A1, A2, B1, and C1 coatings, the maximum protrusion height did not exceed 5 μm.

In turn, for B2, C2, D1, and D2, they were in the range of 10 to 15 μm. It can be observed that the high concentration of Cu^{2+} and the higher deposition current are crucial to the formation of higher protrusions.

It has been reported in the literature that values of roughness parameters of electrodeposited Ni-Cu coatings increase with the higher current density[27,34] and deposition time.[35] At higher current densities and longer deposition times, the surface is rough and the number of cauliflower features increases. This can be explained by the increase in the ion nucleation rate at higher current densities. At high current densities, there is an excess of ions, leading to the uneven growth of the coating in the direction perpendicular to the substrate, creating a rough surface, which was also confirmed by Augustin *et al.*[36] Furthermore, an extension of the electrodeposition time from 15 to 45 minutes at a current density of 10 mA/cm^2 results in significant surface roughness of the coatings. An interesting observation in the present work is that the D1 and D2 coatings obtained from the same bath D exhibit clearly different values of roughness parameters. At a lower current density of 2 A/dm^2, the value of the R_a parameter was several times higher than for the coating obtained with a current density of 4 A/dm^2. However, the value of the R_t parameter was similar. Cauliflower-like structures indicate uneven growth and therefore create a rough surface.[35] In the coatings examined in the present study, the surface roughness increases with increasing Cu content, which is in line with results obtained by Goranova *et al.*[25] They reported that the increase in Ni^{2+} concentration (for the Cu^{2+}:Ni^{2+} molar ratios 1:2, 1:4, 1:6, and 1:8) leads to a smoother surface and an increase in nickel content in the alloy coating at 1 A/dm^2, while at 2 A/dm^2 the dendritic morphology changes to cauliflower-like morphology.[25]

Due to the increase in the catalytic activity of electrocatalysts, a large surface development is necessary and thus a greater active surface area of coatings, which makes the method of electrolytic deposition of Ni-based alloys attractive.

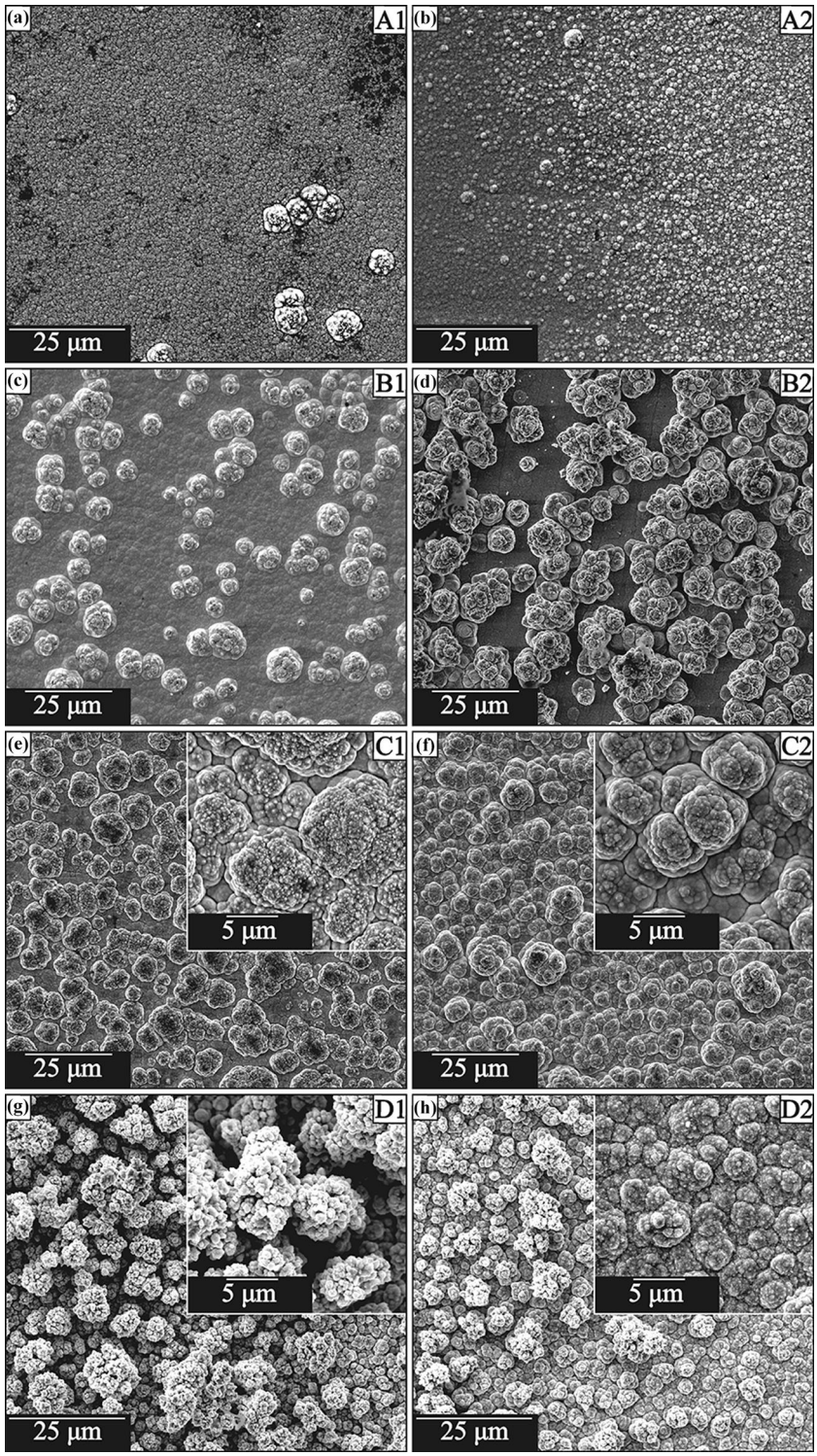

Fig. 1—Surface morphology of the electrodeposited: (*a*) A1, (*b*) A2, (*c*) B1, (*d*) B2, (*e*) C1, (*f*) C2, (*g*) D1, and (*h*) D2 Ni-Cu alloy coatings with higher magnification images in inserts, SEM SE.

B. *Microstructure and Chemical Composition*

Figure 3(a) through (h) shows the cross-section SEM images of the deposited Ni-Cu alloy coatings. The thickness of the coatings was in the range of 10 to 20 μm. The A1 and A2 exhibited a smooth and even surface profile (Figures 3(a) and (b)). With the change of concentration ratio of Cu^{2+}:Ni^{2+} to 1:20 irregularly placed protrusions appeared in the cross-sections of B1 and B2 (Figures 3(c)

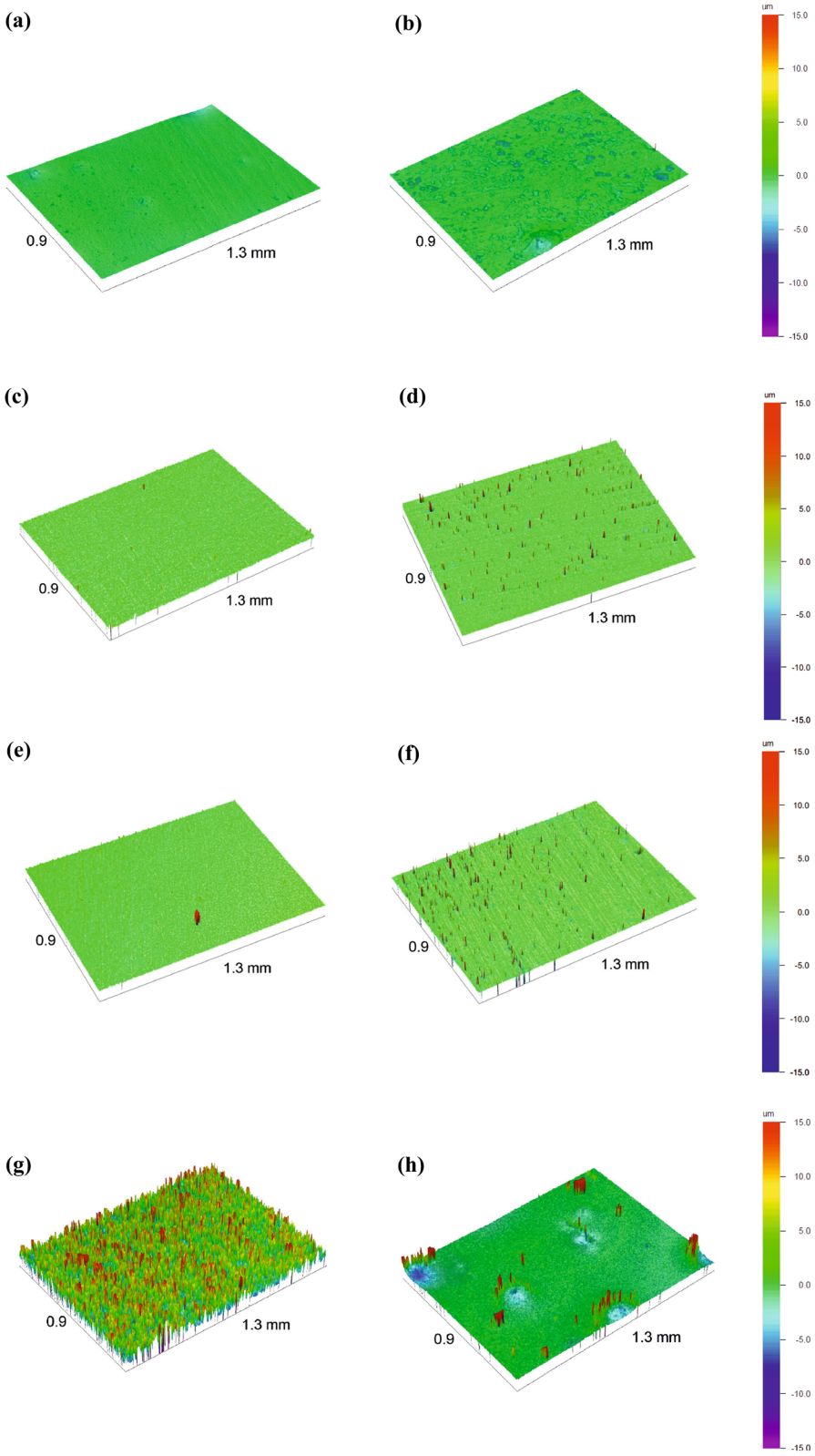

Fig. 2—Roughness maps of the electrodeposited Ni-Cu alloy coatings: (*a*) A1, (*b*) A2, (*c*) B1, (*d*) B2, (*e*) C1, (*f*) C2, (*g*) D1, and (*h*) D2, optical profilometer.

and (d)). For 1:15 ratio, the small microprotrusions in B1 and B2 were regularly placed on the surface of C1 and C2 (Figures 3(e) and (f)). Extensive growth of surface irregularities and formation of large cauliflower-like structures occurred in D1 and D2 coatings electrodeposited from a bath with 1:10 ratio (Figures 3(g) and (h)).

Table III. Roughness Parameters of Ni-Cu Alloy Coatings

Coating	Parameter		
	R_a [μm]	R_q [μm]	R_t [μm]
A1	0.23	0.40	3
A2	0.21	0.37	10
B1	0.50	0.63	10
B2	0.27	0.59	25
C1	0.31	0.48	18
C2	0.46	0.98	28
D1	4.39	5.29	39
D2	0.45	1.19	41

The A1 and A2 coatings had a similar structure to most of the electrodeposited Ni-based coatings with an even thickness, consisting of grains elongated in the direction perpendicular to the substrate.[37,38] Besides, the D1 and D2 coatings were characterized by a hierarchical structure with an evenly distributed nodular structures growing above the mean line of the coating profile to a height less than 5 μm in D1 and less than 10 μm in D2. Results of microstructural investigation of cross-sections are in line with the observations of surface morphology and the profilometry measurements.

TEM microstructural studies were performed for D1 and D2 coatings, which were characterized by a hierarchical structure. The thin foils were prepared from the center part of the thickness of the coatings. Figure 4(a) through (d) shows bright-field TEM images and the corresponding SAED patterns, which reveal a fine-grained microstructure. The grain size histograms are presented in Figures 4(e) and (f), and the ECD values are given in Table IV. In both coatings, the grain diameters were smaller than 300 nm, but the D2 coating was characterized by finer grains with a higher fraction of grains smaller than 100 nm. The mean ECD values for D1 and D2 were equal to 80 ± 49 nm and 60 ± 47 nm, respectively. In turn, the median values of grain diameter were equal to 68 nm and 45 nm. The grain sizes of the Ni-Cu alloy coatings were several orders of magnitude smaller than those obtained in the conventional process[39] but were in a similar range as the electrodeposited Ni-Cu described by Alper *et al.*[3] or other coatings deposited without grain refinement agent additive, such as Ni or Ni-Co.[40–42]

In the D1 and D2 coatings, the rings of the diffraction spots originating from the Ni-Cu solid solution were identified using crystallographic data of γ-Ni (Ni-based solid solution, a = 0.368 nm, space group Fm3m),[43] and γ-$Ni_{0.5}Cu_{0.5}$ (Ni-Cu solid solution, a = 0.3572 nm, space group Fm3m).[44] The difference in the lattice parameter of the γ phase in the analyzed areas of both coatings, resulting from the different concentrations of Cu in Ni, could be a consequence of the cyclic changes of the chemical composition of the bath in the diffusion zone. Although the Cu content in our coatings was lower compared to the study of Goranova,[18] we have achieved a similar surface morphology of the coating which resulted from the microsegregation of Cu rather than the formation of the Cu-rich solid solution.

In addition to the γ phase, weak rings from the intermetallic $L1_0$ NiCu phase were identified (a = 0.330 nm, c = 0.290, space group P4/mmm)[45,46] in both the γ-Ni or γ-$Ni_{0.5}Cu_{0.5}$ areas. The $L1_0$-ordered phase with AB stoichiometry characterized by a primitive tetragonal structure is probably a superlattice derivative of γ-$Ni_{0.5}Cu_{0.5}$ phase. The presence of $L1_0$ phase in electrodeposited Ni-Cu coatings was also observed by Ghosh *et al.*,[46] and in ion beam-evaporated Ni-Cu thin films by Sarrazin *et al.*[45] The $L1_0$ phase is metastable and is quite rarely present in Ni-Cu alloys. Its electrodeposition requires the formation of high energy nucleation sites due to high local overpotential and thus is slower than the deposition of the disordered γ solid solution. The process of $L1_0$ formation might probably be accelerated by temporary local inhibition of kink sites by citrate anions. The specific crystallization requirement causes $L1_0$ grains to be much smaller than γ phase.[46]

The average concentration of Cu in the coatings determined by EDS is given in Table V.

An increase in the average Cu content was observed due to an increase in the concentration of Cu^{2+} ions in the electrolytic bath. Furthermore, a lower Cu content was observed in all samples deposited at 4 A/dm^2 than 2 A/dm^2.

However, the results of phase identification by electron diffraction analysis indicate the local variations in the Ni and Cu concentrations. Therefore, quantitative EDS microanalysis was performed on the cross-section of the coatings. Figure 5(a) through (d) shows the quantitative chemical composition maps that reveal the concentration of Cu, superimposed on the SEM cross-section images of the coatings. The locations of the point EDS microanalysis are marked. The color scale was selected according to the concentration ranges from minimum to maximum of Cu content in the examined area, to emphasize the local fluctuations in chemical composition. Therefore, the similar colors in Figures 5(a) through (d) do not correspond to the similar Cu concentrations. The distribution of Ni and Cu is inhomogeneous for all coatings. A higher Cu content was observed in the protrusions.

In A1 and D1 coatings, the differences in Cu distribution revealed its segregation to dendrites, and a significant increase in the Cu content was observed in microprotrusions (Figures 5(a) and (c)). Moreover, the formation of microprotusions was preceded by the decrease in the Cu content (Figures 5(c) and (d)). This result confirms that the intensification of dendritic growth occurs when the local concentration of Cu^{2+} ions in the bath decreases.

In the D1 and D2 coatings, a depletion of the diffusion zone in the Cu^{2+} ions during deposition caused more developed surface morphology and formation of higher microprotrusions in D2 than D1. On the contrary, in the case of A1 and A2 coatings, the concentration of Cu ions in the bath was low and only a limited effect of dendritic growth on the microstructure was observed (Figures 5(a) and (b)). The A2 coating was

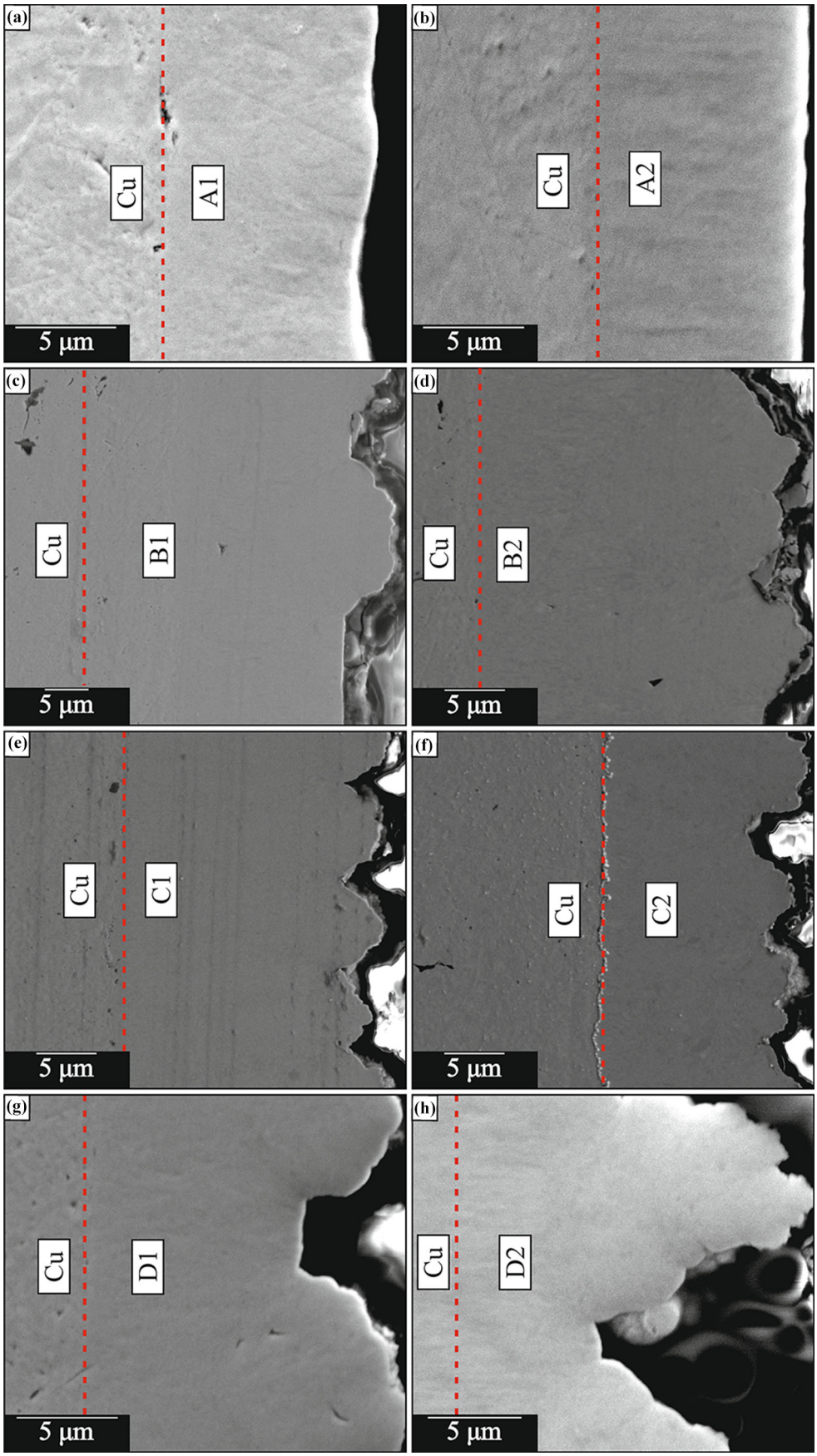

Fig. 3—Microstructure of (*a*) A1, (*b*) A2, (*c*) B1, (*d*) B2, (*e*) C1, (*f*) C2, (*g*) D1, and (*h*) D2 coatings observed in cross-section images, SEM, SE.

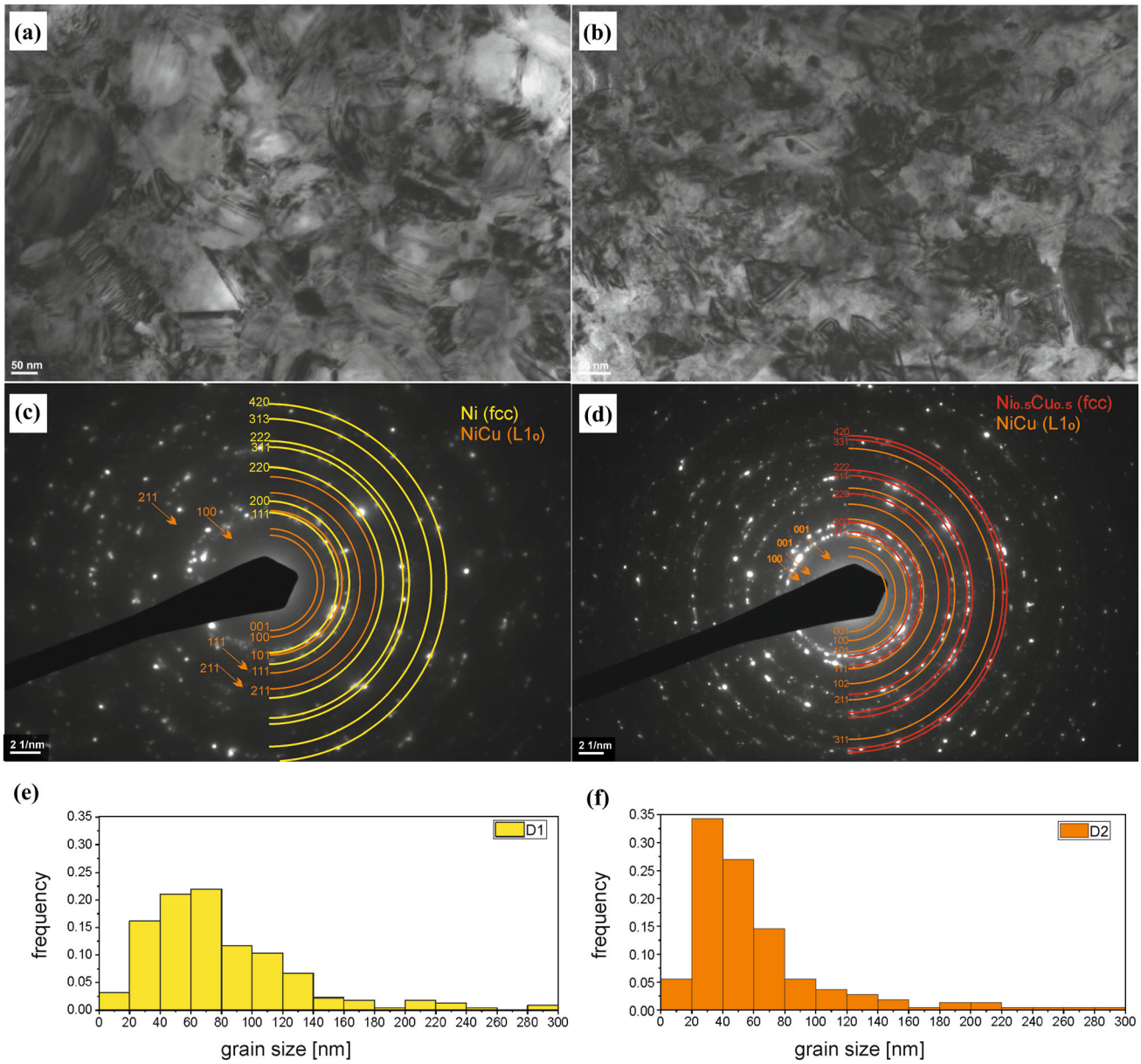

Fig. 4—TEM bright-field images of (*a*) D1 and (*b*) D2 coatings with corresponding SAED patterns and their solution for (*c*) Ni and $L1_0$ phase in D1 and (*d*) $Ni_{0.5}Cu_{0.5}$ and $L1_0$ phase in D2, as well as (*e*, *f*) grain size distribution in D1 and D2.

Table IV. ECD Range, Mean ECD With Its Standard Deviation ($\overline{ECD} \pm SD$) and Median of ECD in D1 and D2 Coatings

Coating	Parameter		
	ECD Range [nm]	$\overline{ECD} \pm$ SD [nm]	Median of ECD [nm]
D1	10 to 289	80 ± 49	68
D2	13 to 284	60 ± 47	45

characterized by a more even surface than A1 (electrodeposited at lower current density), which might be connected with a lower deposition rate and a higher concentration of Cu ions in the diffusion layer or/and by overpotential. On the basis of the results of the surface morphology and roughness, it can be assumed that the growth of coatings deposited from baths B and C will proceed in an analogous pattern.

Higher current density during electrodeposition caused a lower concentration of Cu in the electrodeposited coatings, which was caused by the higher electrodeposition rate and lower average concentration

of Cu ions in the diffusion layer. It is in line with the literature data on electrodeposition using citrate baths, which show that Cu is usually reduced under the control of mass transport, while Ni is under the control of activation over a wide range of potentials.[18,47,48] Moreover, it was revealed that with increasing current density, the Ni content in Ni-Cu alloys obtained from citrate-based baths increases.[2,18,23,47]

The microsegregation of Cu in coatings is related to the co-deposition mechanism of Ni^{2+} and Cu^{2+} ions. The deposition behavior of Ni^{2+} and Cu^{2+} in a citrate bath is well known.[34,49] Preferential reduction of Cu^{2+} over Ni^{2+} ions causes the depletion of Cu^{2+} ions in the diffusion layer and thus the dendritic growth caused by mass limitation,[50,51] which was confirmed by the higher concentration of Cu on the surface of the coating. During electrodeposition, Cu^{2+} ions are reduced at microprotrusions, while Ni^{2+} ions are discharged in more recessed parts of the coating. Similar observations are described by Deo *et al.*[35]

Table V. Average Chemical Composition of Electrodeposited Ni-Cu Coatings

Coating	Average Concentration of Cu ± Standard Deviation [Weight Percent]
A1	6.7 ± 1.1
A2	4.7 ± 1.0
B1	8.4 ± 3.3
B2	6.9 ± 3.9
C1	13.2 ± 3.8
C2	8.3 ± 4.5
D1	18.3 ± 5.9
D2	11.6 ± 9.0

Based on the microstructural and compositional studies, a three-stage scheme for the formation of hierarchical surface morphology in Ni-Cu coatings is proposed in Figure 6. At the start of electrodeposition, the chemical composition of the bath is similar in the diffusion zone and the bulk electrolyte. Therefore, in the first stage, the thin inner zone of a coating with uniform chemical composition and smooth surface is electrodeposited. As a result of the depletion of Cu^{2+} ions in the diffusion layer, in the second stage, Cu^{2+} ions are more likely to be deposited in the dendritic microprotrusions, giving rise to the shaping of a surface development. During the third stage, regularly spaced microprotrusions with a higher Cu content grow faster than adjacent areas, deposited from a bath depleted in Cu^{2+} ions, and consequently, the outer zone of a coating with a hierarchical morphology is formed.

The presented scheme is based on the microstructural and compositional studies performed on the cross-sections of the coatings and therefore gives a new input into the detailed examination of the growth mechanism of Ni-Cu coatings. Therefore, it is a complement to the previous model presented in Reference 18, which was

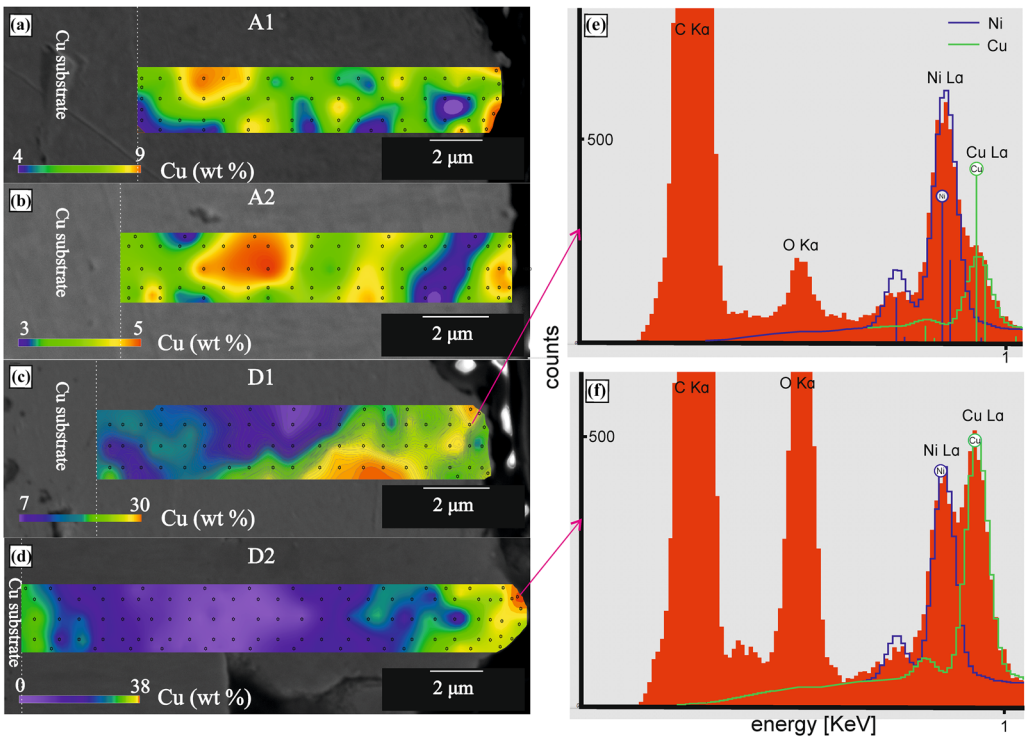

Fig. 5—Concentration maps of Cu in (*a*) A1, (*b*) A2, (*c*) D1, and (*d*) D2 coatings superimposed with their SEM SE cross-sections images. The locations of point EDS microanalysis are marked. Fragments of the experimental EDS spectra acquired in the (*e*) medium and (*f*) high Cu concentration areas with the calculated curves showing the deconvolution of the Ni-Lα (in blue) and Cu-Lα (in green) peaks are also given (Color figure online).

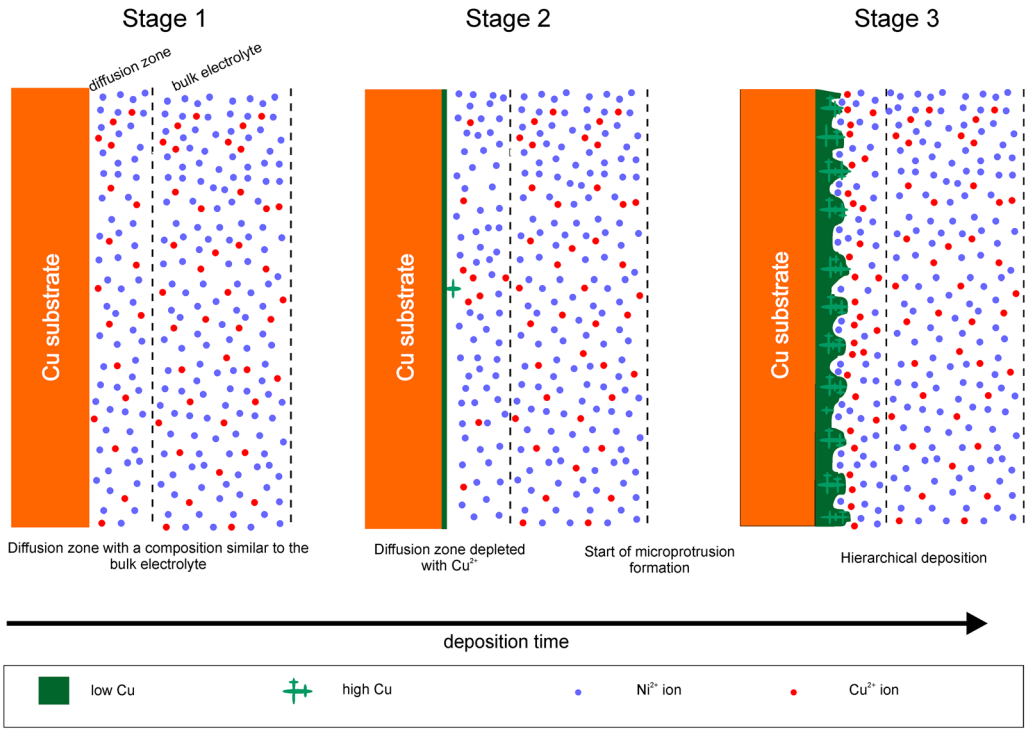

Fig. 6—Scheme of the formation of hierarchical morphology of Ni-Cu coatings: stage (1), the chemical composition of the bath is similar in the diffusion zone and the bulk electrolyte; stage (2), as a result of the depletion of Cu^{2+} ions in the diffusion layer, formation of microprotrusions is initiated; and stage (3), microprotrusions with higher Cu content separated by areas depleted with Cu are created.

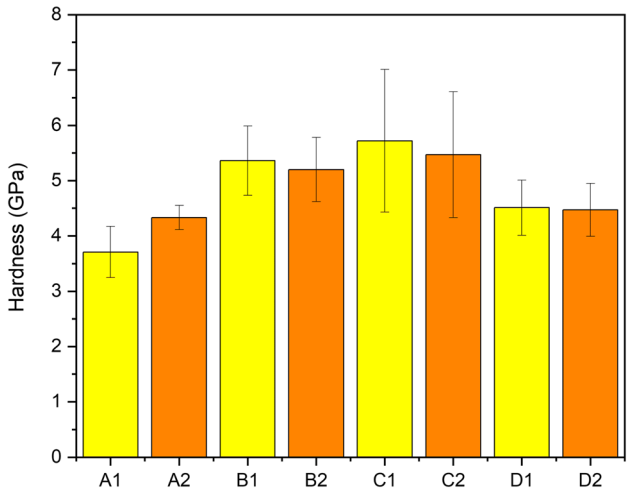

Fig. 7—Microhardness of electrodeposited Ni-Cu coatings.

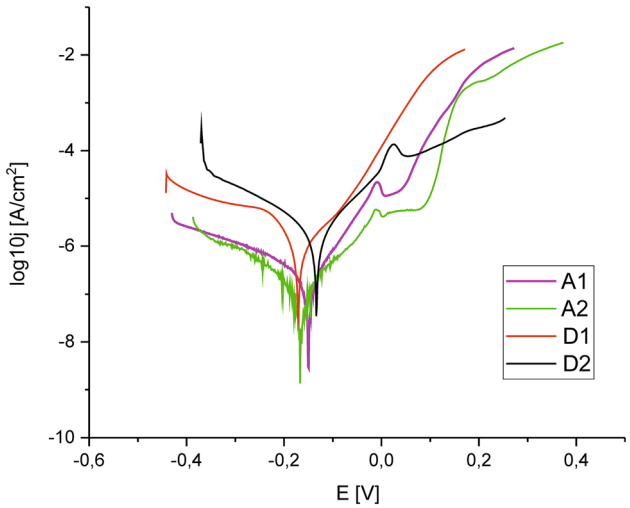

Fig. 8—Potentiodynamic curves of electrodeposited Ni-Cu alloy coatings.

postulated on the basis of the surface morphology and local chemical analysis of the areas near the surface.

C. *Microhardness*

The results of the microhardness measurements are given in Figure 7. The bars show the mean values of 10 microhardness measurements and the error bars showing the standard deviation are marked. The average values and their standard deviations indicate that the differences in the microhardness of the B1, B2, C1, and C2 coatings are slight, but it can be concluded that the hardness of these coatings is greater than A1, A2, D1, and D2.

The highest microhardness was reached for coatings obtained from baths B and C. The lowest microhardness was observed for coatings obtained from bath A with the lowest Cu content in the electrolyte. However, for coatings obtained from baths with the highest copper content, the microhardness was slightly higher than that

Table VI. Results of Measurements of Electrochemical Parameters Determined During the Corrosion Resistance Test in 3 Pct NaCl Solution

Coating	OCP [V]	Corrosion Potential E_{cor} [V]	Corrosion Current Density j_{corr} [A/cm^2]
A1	− 0.131	− 0.147	4.04×10^{-7}
A2	− 0.088	− 0.180	8.52×10^{-8}
D1	− 0.144	− 0.170	1.41×10^{-6}
D2	− 0.074	− 0.131	2.72×10^{-6}

obtained from bath A. The results of microhardness measurements were similar to the literature reports obtained for Ni-based coatings.[52–56]

In the coatings obtained from electrolytic baths B and C, it was observed that with the increase of the Cu content in the coatings, the microhardness increased compared to coatings with a lower copper concentration in the coatings. It is also closely related to the current density of deposition, the deposition at 2 A/dm^2 increases the microhardness in these coatings compared to the deposition at 4 A/dm^2. It is well known that the hardness of the material depends on the grain size, so the smaller the grain size, the bigger is the fraction of grain boundaries in the volume, which impede the dislocations' movement.[57] It is also worth noting that the electrodeposited alloys with finer grain size might be characterized by higher compactness and lower porosity.[8]

However, B1 and B2 coatings are characterized by lower microhardness than C1 and C2 coatings, indicating an influence of the solid solution mechanism due to the dissolution of Cu atoms in Ni matrix. The presented data are consistent with the study of Epstein and Carlson[58] and Dai *et al.*[59] who confirmed that the mechanical properties of the Ni-Cu alloys increase due to solid solution with Cu content up to 32 pct. They showed that this is related with both the solid solution strengthening and grain refinement.

In our study, we observed local differences in microhardness in the coatings, which are the result of heterogeneous growth, and correlate well with the surface morphology. However, the heterogeneous hierarchical structure is also associated with the heterogeneities in the chemical composition and grain size, and thus the higher values of the microhardness are related both with the dissolution of Cu in the Ni matrix and the grain refinement.

D. *Electrochemical Studies*

Figure 8 shows the potentiodynamic polarization curves for Ni-Cu coatings in 3 pct NaCl solution and the corrosion parameters are presented in Table VI. OCP values were in the range from − 0.144 to − 0.074 V. The E_{corr} values were in the narrow range between − 0.180 and − 0.131 V and were slightly higher than OCP. No differences in OCP and E_{corr} related to the chemical composition were observed.

The corrosion current density j_{corr} values were higher about a decade for the coatings obtained from the D bath than the A bath. Such differences in corrosion current were caused by the higher surface development of the D1 and D2 coatings. Furthermore, in the polarization curves of A1, A2, and D2, the passive area was in the range of potential from 0.01 to 0.08 V. The lack of passivation of D1 might be related to a higher surface roughness of that coating.

The obtained values of corrosion parameters of A1 and A2 coatings demonstrate their very good corrosion resistance and self-passivation behavior in the presence of chloride ions. However, the higher Cu content observed on the surface may cause a less electronegative corrosion potential of the Ni-Cu than the pure Ni obtained in our previous work,[60] which makes the alloy coatings less susceptible to electrochemical corrosion.

The deterioration of corrosion resistance due to the higher roughness of the surface is obvious, well known, and described in many works, *e.g.* References 61–64. However, high surface roughness is desirable in materials for application as catalytic materials[65–68] and OER/HER electrodes. Therefore, the hierarchical coatings obtained in this study are characterized by a favorable combination of surface roughness and electrochemical properties in terms of their prospective application.

IV. CONCLUSIONS

In this study, Ni-Cu coatings with hierarchical surface morphology consisting of ordered microprotrusions were deposited through single-step electrodeposition. The influence of deposition conditions on the surface morphology and roughness, microstructure, chemical composition, microhardness, and electrochemical properties of Ni-Cu coatings was investigated.

The results showed that the concentration of Cu^{2+} ions in the electrolyte and the current density have a significant influence on the surface morphology and roughness. We have found that uniform hierarchical structure starts to form for the Cu^{2+}:Ni^{2+} ratio greater than 1:15.

The formation of ordered Cu-rich microprotrusions is related to the kinetics of the reduction of Ni^{2+} and the Cu^{2+} ions and the dendritic growth of the coating. Moreover, TEM investigations revealed that the microsegregation of Cu in the coatings results in local differences in the phase composition. The fine-grained microstructure consists on the γ phase solid solution with lattice parameter varied with Cu concentration, as

well as the ordered intermetallic NiCu phase with the $L1_0$ structure. It was demonstrated that the coatings exhibit a combination of a high microhardness and good corrosion resistance. Because of the unique morphology, microstructure, and promising properties, the developed Ni-Cu coatings are expected to be useful for electrode and catalytic applications.

ACKNOWLEDGMENTS

The authors thank Prof. Slawomir Kac (AGH UST) for providing access to the facilities for SEM analysis, hardness, and roughness measurements.

FUNDING

The study was supported by AGH UST Project No. 16.16.110.663.

CONFLICT OF INTEREST

The authors declare that they have no conflict of interest.

OPEN ACCESS

This article is licensed under a Creative Commons Attribution 4.0 International License, which permits use, sharing, adaptation, distribution and reproduction in any medium or format, as long as you give appropriate credit to the original author(s) and the source, provide a link to the Creative Commons licence, and indicate if changes were made. The images or other third party material in this article are included in the article's Creative Commons licence, unless indicated otherwise in a credit line to the material. If material is not included in the article's Creative Commons licence and your intended use is not permitted by statutory regulation or exceeds the permitted use, you will need to obtain permission directly from the copyright holder. To view a copy of this licence, visit http://creativecommons.org/licenses/by/4.0/.

REFERENCES

1. E. Pellicer, A. Varea, S. Pané, K.M. Sivaraman, B.J. Nelson, S. Suriñach, M.D. Baró, and J. Sort: *Surf. Coat. Technol.*, 2011, vol. 205, pp. 5285–93.
2. I. Baskaran, T.S.N.S. Narayanan, and A. Stephen: *Mater. Lett.*, 2006, vol. 60, pp. 1990–95.
3. M. Alper, H. Kockar, M. Safak, and M.C. Baykul: *J. Alloys Compd.*, 2008, vol. 453, pp. 15–19.
4. E. Beltowska-Lehman, E. Chassaing, and K.V. Quang: *J. Appl. Electrochem.*, 1991, vol. 21, pp. 606–11.
5. P. Calleja, J. Esteve, P. Cojocaru, L. Magagnin, E. Vallés, and E. Gómez: *Electrochim. Acta.*, 2012, vol. 62, pp. 381–89.
6. R. Solmaz, A. Döner, and G. Kardaş: *Electrochem. commun.*, 2008, vol. 10, pp. 1909–11.
7. K. Agarwal, M. Kumar, V. Malladi, S.R.K. Balasubramaniam, and R. Balani: *JOM J. Miner. Met. Mater. Soc.*, 2010, vol. 62, pp. 88–92.
8. S.K. Ghosh, A.K. Grover, G.K. Dey, and M.K. Totlani: *Surf. Coat. Technol.*, 2000, vol. 126, pp. 48–63.
9. T.A. Green, A.E. Russell, and S. Roy: *J. Electrochem. Soc.*, 1998, vol. 145, pp. 875–81.
10. S. Roy: *J. Electrochem. Soc.*, 1994, vol. 141, pp. 1509–16.
11. N.D. Nikolić, P.M. Živković, N. Elezović, and U. Lačnjevac: *J. Solid State Electrochem.*, 2020, vol. 24, pp. 1615–24.
12. X. Yu, J. Yang, X. Ren, and Z. Sui: *Membranes (Basel).*, 2021, vol. 11, pp. 1–13.
13. X. Yu and Z. Yuan: *Metall. Mater. Trans. B.*, 2019, vol. 50, pp. 587–94.
14. X. Yu, M. Wang, Z. Wang, X. Gong, and Z. Guo: *J. Phys. Chem. C.*, 2017, vol. 121, pp. 16792–16802.
15. E. Hatami, A. Toghraei, and G.B. Darband: *Int. J. Hydrogen Energy.*, 2021, vol. 46, pp. 9394–9405.
16. P. Salehikahrizsangi, K. Raeissi, F. Karimzadeh, L. Calabrese, and E. Proverbio: *Appl. Surf. Sci.*, 2020, vol. 520, pp. 1–9.
17. Z. Chen, C. Zhu, M. Cai, X. Yi, and J. Li: *Appl. Surf. Sci.*, 2020, vol. 508, pp. 1–10.
18. D. Goranova, R. Rashkov, G. Avdeev, and V. Tonchev: *J. Mater. Sci.*, 2016, vol. 51, pp. 8663–73.
19. F. Wolfart, B.R. Brito, L.F. Marchesi, and M. Vidotti: *J. Braz. Chem. Soc.*, 2017, vol. 28, pp. 1732–40.
20. X. Zhang, T. Wang, L. Ma, Q. Zhang, Y. Yu, and Q. Liu: *Catal. Commun.*, 2013, vol. 33, pp. 15–19.
21. A.A. Smirnov, S.A. Khromova, O.A. Bulavchenko, V.V. Kaichev, A.A. Saraev, S.I. Reshetnikov, M.V. Bykova, L.I. Trusov, and V.A. Yakovlev: *Kinet. Catal.*, 2014, vol. 55, pp. 69–78.
22. Q. Yu, Z. Zeng, W. Zhao, M. Li, X. Wu, and Q. Xue: *Colloids Surf. A Physicochem. Eng. Asp.*, 2013, vol. 427, pp. 1–6.
23. M. Sundaram, A.B. Kamaraj, and G. Lillie: *Procedia CIRP.*, 2018, vol. 68, pp. 227–31.
24. M.A. Khan, H. Zhao, W. Zou, Z. Chen, W. Cao, J. Fang, J. Xu, L. Zhang, and J. Zhang: *Electrochem. Energy Rev.*, 2018, vol. 1, pp. 483–530.
25. D. Goranova, G. Avdeev, and R. Rashkov: *Surf. Coat. Technol.*, 2014, vol. 240, pp. 204–10.
26. M. Haciismailoglu and M. Alper: *Surf. Coat. Technol.*, 2011, vol. 206, pp. 1430–38.
27. U. Sarac, R.M. Öksüzoğlu, and M.C. Baykul: *J. Mater. Sci. Mater. Electron.*, 2012, vol. 23, pp. 2110–16.
28. P.J. Potts: *A Handbook of Silicate Rock Analysis*, Chapman and Hall, New York, 1987, pp. 336–37.
29. Y. Xu, M. Yamazaki, and P. Villars: *Jpn. J. Appl. Phys.*, 2011, vol. 50, pp. 1–5.
30. H. Kockar, M. Bayirli, and M. Alper: *Appl. Surf. Sci.*, 2010, vol. 256, pp. 2995–99.
31. Ö. Öztop, G.H. Ağaoğlu, and G. Orhan: *Surf. Eng. Appl. Electrochem.*, 2019, vol. 55, pp. 410–17.
32. R.S. Yang, Q.S. Fu, M.T. Li, and Y.Z. Jin: *Adv. Mater. Res.*, 2014, vol. 910, pp. 11–14.
33. H. Nady and M. Negem: *Zeitschrift fur Phys Chemie.*, 2016, vol. 231, pp. 1–20.
34. R.Y. Ying, P.K. Ng, Z. Mao, and R.E. White: *J. Electrochem. Soc.*, 1988, vol. 135, pp. 2964–71.
35. Y. Deo, S. Guha, K. Sarkar, P. Mohanta, D. Pradhan, and A. Mondal: *Appl. Surf. Sci.*, 2020, vol. 515, pp. 1–12.
36. A. Augustin, K.R. Udupa, and K.U. Bhat: *Perspect. Sci.*, 2016, vol. 8, pp. 472–74.
37. A. Shibata, H. Noda, M. Sone, and Y. Higo: *Thin Solid Films.*, 2010, vol. 518, pp. 5153–58.
38. V.G. Shadrow, T.A. Tochitskii, and A.V. Boltushkin: *Cryst. Res. Technol.*, 1993, vol. 28, pp. 157–61.
39. W.D. Cao, M.W. Lee, and R.L. Kennedy: *Scr. Metall. Mater.*, 1993, vol. 28, pp. 955–60.
40. B. Li, T. Mei, D. Li, and S. Du: *Ultrason. Sonochem.*, 2019, vol. 58, pp. 1–9.
41. T. Ratajski, I. Kalemba-Rec, P. Indyka, S. Kąc, M. Kot, and B. Dubiel: *Mater. Charact.*, 2018, vol. 142, pp. 478–91.
42. A.W. Thompson and H.J. Saxton: *Metall. Trans.*, 1973, vol. 4, pp. 1599–1605.

43. J.W. Cable and Y. Tsunoda: *J. Magn. Magn. Mater*., 1995, vol. 140–144, pp. 93–94.
44. R.P. Van Ingen, R.H.J. Fastenau, and E.J. Mittemeijer: *J. Appl. Phys*., 1994, vol. 76, pp. 1871–83.
45. C. Sarrazin, R.J. Gaboriaud, and J.P. Rivière: *Phys. Status Solidi*., 1988, vol. 107, pp. 867–71.
46. S.K. Ghosh, A.K. Grover, G.K. Dey, U.D. Kulkarni, R.O. Dusane, A.K. Suri, and S. Banerjee: *J. Mater. Res*., 2006, vol. 21, pp. 45–61.
47. S. Rode, C. Henninot, and M. Matlosz: *J. Electrochem. Soc*., 2005, vol. 152, pp. C248-254.
48. E. Chassaing, K.V. Quang, and R. Wiart: *J. Appl. Electrochem*., 1987, vol. 17, pp. 1267–80.
49. T.B. Field, J.L. McCourt, and W.A.E. McBryde: *Can. J. Chem*., 1974, vol. 52, pp. 3119–24.
50. D. Landolt: *Electrochim. Acta*., 1994, vol. 39, pp. 1075–90.
51. T. Watanabe: *Nano-plating: Microstructure Control Theory of Plated Film and Data Base of Plated Film Microstructure*, 1st ed. Elsevier Science, Amsterdam, 2004, pp. 37–38.
52. A. Varea, E. Pellicer, S. Pané, B.J. Nelson, S. Suriñach, M.D. Baró, and J. Sort: *Int. J. Electrochem. Sci*., 2012, vol. 7, pp. 1288–1302.
53. M. Trzaska and G. Cieślak: *Compos. Theory Pract*., 2014, vol. 14, pp. 50–53.
54. A.A. Maizelis, B.I. Bairachniy, L.V. Trubnikova, and B.A. Savitsky: *Funct. Mater*., 2012, vol. 19, pp. 238–44.
55. J.C. Hsu and K.L. Lin: *Thin Solid Films*., 2005, vol. 471, pp. 186–93.
56. P. Ledwig, M. Kac, A. Kopia, J. Falkus, and B. Dubiel: *Materials (Basel)*., 2021, vol. 14, pp. 1–16.
57. N.J. Petch: *I. Iron Steel Inst*., 1953, vol. 174, pp. 25–28.
58. S.G. Epstein and O.N. Carlson: *Acta Metall*., 1965, vol. 13, pp. 487–91.
59. P.Q. Dai, C. Zhang, J.C. Wen, H.C. Rao, and Q.T. Wang: *J. Mater. Eng. Perform*., 2016, vol. 25, pp. 594–600.
60. P. Ledwig and B. Dubiel: *Arch. Metall. Mater*., 2017, vol. 62, pp. 2455–60.
61. G. Ghosh, A. Sidpara, and P.P. Bandyopadhyay: *Surf. Coat. Technol*., 2019, vol. 378, pp. 1–16.
62. S.G. Croll: *Prog. Org. Coat*., 2020, vol. 148, pp. 1–14.
63. R. Walter and M.B. Kannan: *Mater. Des*., 2011, vol. 32, pp. 2350–54.
64. A.S. Toloei, V. Stoilov, and D.O. Northwood: *WIT Trans. Eng. Sci*., 2013, vol. 77, pp. 193–204.
65. R.K. Shervedani and A. Lasia: *J. Appl. Electrochem*., 1999, vol. 29, pp. 979–86.
66. I. Kim, G. Park, and J.J. Na: *Int. J. Heat Mass Transf*., 2019, vol. 138, pp. 916–22.
67. I. Kim, Y. Yang, and G. Park: *Acta Astronaut*., 2020, vol. 166, pp. 260–69.
68. I. Herraiz-Cardona, E. Ortega, J.G. Antón, and V. Pérez-Herranz: *Int. J. Hydrogen Energy*., 2011, vol. 36, pp. 9428–38.

Publisher's Note Springer Nature remains neutral with regard to jurisdictional claims in published maps and institutional affiliations.